A Study on Data-driven Methods for Selection and Evaluation of Beam Subsets in 5G NR

Nic Ekman & Ilias Theodoros Skordas

Ericsson Supervisor / LTH Supervisor / Examiner

Marcus Davidsson Björn Landfeldt Mats Gustafsson

LUND UNIVERSITY

Department of Electrical Engineering

MSc Thesis

Department of Electrical Engineering
Lund University
Box 118
SE-221 00 LUND
Sweden

Printed in Sweden by E-Husets Tryckeri.
Lund 2022

Abstract

5G New Radio is the next generation of mobile networks and it comes with promises of ultra-high speeds, ultra-high reliability and ultra-low latency. This has posed a challenge for the engineers entrusted with the task of finding solutions which could fulfil the specification, and as a result, some promising areas have received increased attention in recent years. Signal processing techniques like directional transmission and reception, also referred to as beamforming, is believed to be a key area of advancement to meet the requirements. The general benefit of applying beamforming is to concentrate the power of a signal in a given direction, which also translates to a smaller area of coverage on the ground surface. As a user traverses the area surrounding a base station, it will thus need to keep an updated image of the radio environment including available beams for transmission and reception. This is done through a frequent and periodic synchronization signal procedure which, partially due to carrier aggregation, intensifies the workload put on the often battery powered user equipment as it continuously updates and stores state variables related to available physical channels. In order to reduce required processing power and cache memory usage in the user equipment, telecommunications engineers have introduced beam subsets which each user may operate on rather than the full set of available beams.

This report investigates purely data-driven and machine learning based alternatives to the current, static, implementation responsible for selecting and evaluating beam subsets with the goal of mitigating the downsides posed by not considering all available channels, as is the case with any such subset strategy.

The results show that the current static implementation of the subset selector can be improved in terms of reducing the selected subsets which do not include the widebeam of highest signal strength at a cost of more frequent subset updates, which are of relevance for distributed systems where such configurations take place over the air interface. A probabilistic approach involving a Markov Chain yielded the greatest benefit at the highest subset update cost, while a Machine Learning approach involving a Random Forest Regressor offers a smaller improvement at a much lower cost relative to the Markov method. A subset evaluation technique involving a Multi-Layer Perceptron classifier yielded promising results, being able to

detect 76.8% of subsets not including the strongest widebeam. Another evaluation technique based on a convolutional neural network resulted in accuracies of up to 95% based on various different image inputs. Furthermore, it was shown via experiments performed on the Markov method that the frequency of selected subsets which did not include the best widebeam decrease exponentially with an increasing subset size.

Acknowledgements

We would like to extend our appreciation to the people who helped make this project possible. Thank you to Filip Johansson and Markus Ernstsson for your expert input on the inner workings of NR. Likewise, to Marcus Davidsson, with special recognition for being so attentive throughout the whole project despite your overflowing calendar. Thank you to Mattias Swenje for valuable guidance on teamwork, organization and planning, to Björn Landfeldt for your flexibility and input on the report and to Mats Gustafsson for examining the project on behalf of The Faculty of Engineering at Lund University.

Contents

List of Figures

List of Tables

1

Introduction

5G New Radio (NR) is the next generation of mobile networks and it comes with marketing promises of ultra-high speeds, ultra-high reliability and ultra-low latency. [Ericsson, 2022b] This has posed a challenge for the engineers entrusted with the task of finding solutions that fulfil these promises while also satisfying the 3GPP specification, and as a result, some promising areas have received increased attention in recent years. [Ericsson, 2022a] In order to solve these problems, the industry focus has shifted to frequency bands located far above those of previous generations along with techniques like Massive Multiple-Input-Multiple-Output (MIMO) and intelligent beamforming. This report aims to provide a contribution to this new area of research by investigating the possibility to save resources and improve performance by managing the available physical channels efficiently using data-driven methods including, but not limited to, Machine Learning (ML).

1.1 Project Motivation

A theoretical environment without any obstacles provides what is referred to as line-of-sight (LOS) conditions, meaning that any signal sent between User Equipment (UE) and Base Station (Next Generation Node B, gNB) travels in a straight line between transmitter and receiver. The analog beamforming performed at gNB is configured to cover a certain area on the ground commonly referred to as a sector. In perfect LOS conditions, the optimal choice of subset would be that which surrounds the UE in a circle-like structure since these widebeams would always yield the highest Reference Signal Received Power (RSRP) when measured by the UE. Matters become more complicated when introducing obstacles as they give rise to reflections and shadowing, complicating the mapping between the theoretical grid and real coverage. In LOS conditions, the optimal subset can be easily identified as the geographical neighbors of the UE. In non-line-of-sight (NLOS), it makes more sense to talk about neighbors in terms of signal strength.

In an effort to enable dynamic channel selection to adjust for movement and disturbances, the UE continuously performs measurements on so-called Tracking

Reference Signals (TRS), which are sent for each carrier in each widebeam, and stores them in cache memory. Since this operation has to be done for each carrier in each widebeam, the required cache memory and Digital Signal Processor (DSP) processing power on the UE side becomes a limiting factor. Therefore, the UE will report its TRS limit to gNB at connection setup and gNB will calculate how many widebeams the TRS limit corresponds to. If the TRS limit corresponds to a lower number than the number of widebeams in the cell, gNB is forced to instead assign a subset of widebeams for the UE to keep track of. This subset may then be updated during the full duration of the connection. The selection of which widebeams to include in a given subset is crucial to the user experience with the ultimate goal of always including the highest RSRP widebeam in the subset.

The current procedure responsible for handling widebeam selection keeps track of four static subsets of all available widebeams in a cell. Specifically, the cell consists of 24 widebeams which are divided into four overlapping subsets of size 14 (the size is based on the number derived from the TRS limit of the device used in experiments). Furthermore, the UE measures the channel state information of all widebeams in its assigned subset, but only the top four are reported back to gNB.

In an effort to optimize the user experience with respect to the fixed-size subset condition posed by the UE, this report aims to investigate alternative methods to the subset member selection algorithm that is currently used in several Radio Access Network (RAN) components offered by Ericsson. As a complement to this, methods for evaluating a given subset will also be investigated with the aim of laying the groundwork for future, more sophisticated subset selectors which could theoretically be feedback driven. The set of key performance indicators to be used are presented in Section 1.3.

To summarize, the project objectives are as follows:

- Evaluate how the baseline subset selector performs with respect to the below specified KPIs.
- Develop and benchmark alternative methods of subset selection that select subset members dynamically, based on data gathered from the radio environment.
- Investigate the idea of utilizing Machine Learning to evaluate whether or not the highest RSRP beam is present in a measurement report of a given subset.

1.2 Delimitations

User data from real world deployments are protected by data protection laws such as GDPR around the globe. To avoid handling of sensitive data and save time, it was decided that an internal simulator was to be used to produce the data necessary

to perform all experiments within this project. It must thus be said that any results and conclusions presented in this report apply to the performance of the internal simulator and not necessarily the real-world products it was set up to simulate. It is however assumed, due to the scale at which the simulator is used to conduct Ericsson internal research, that any present discrepancies between the simulation and the real world are negligible with respect to this project.

Furthermore, it was decided that the effectiveness of any algorithms produced by the authors be evaluated against a Python implementation of the real product behavior. The sections of the code responsible for subset selection in the product source-code will hence be implemented in Python along with logging functionality needed to extract information about the performance.

1.3 Key Performance Indicators (KPI)

The first key performance indicator related to selection of physical channel is the frequency at which subsets are updated as this procedure requires an Radio Resource Control (RRC) reconfiguration exchange, costing bandwidth. This indicator will be quantified as the frequency of *subset switches*. The second primary indicator is the quality of the selected subset itself. There are several ways of quantifying the quality, but the most indicative one was determined to be if the highest RSRP beam in the cell is part of the subset or not, as the best beam in the subset constitutes the upper limit of the channel quality. The case where the best global beam is not included in the selected subset will be referred to as a *beam miss* in this report. The third indicator, *average RSRP* over time during the connection, is interesting as it indicates the macro effect of the micromanagement that is selection of individual subsets. Similar to the frequency of subset switches, it should be mentioned that the frequency of beam switches does also come at a cost of synchronization bandwidth, but this generally accepted as the end goal of subset management is to always make use of the highest RSRP beam.

1.4 Previous Work

The topic of beam management is related to selection of widebeams, but also so-called *narrowbeams* or *traffic beams* which are carriers that further divide and refine the areas covered by each widebeam. A previous study [Wang, 2021] conducted under supervision of Ericsson successfully showed the possibility of using machine learning to reduce the number of synchronization signals needed to adequately select such a traffic beam in LOS conditions. The idea to also investigate machine learning as a method to improve widebeam selection in NLOS conditions, which is the topic of this report, was part of the same initiative to optimize resource allocation in beam management. The similarities between the projects allowed the authors (*us*) to re-use parts of the simulator logging functionality implemented as a

part of Wang's project. Furthermore, the workflow of using the internal radio environment simulator to evaluate performance offline by using MATLAB for sanitation and Python with Scikit Learn for ML applications was inspired by several previous projects conducted by M.Sc. students at Ericsson.

It should also be mentioned that beam subset selection based on data gathered from radio environments has been theorized and published in the form of a patent application by Patel et al., on behalf of Ericsson. The suggested architecture involves a central node configured to, via beamforming, transmit signals to a number of users and selecting a suitable beam subset based on the predicted trajectory of the user device. [Patel et al., 2020] This material served as an inspiration to the objectives presented in this report.

The application of machine learning in telecommunications has been studied extensively in various publications. A study conducted by Sim et al. developed an algorithm for millimeter wave beam selection which build upon the idea of estimating the power delay profile of a sub-6 GHz channel using a dense neural network. After testing said algorithm in both simulated environments and real-world experiments the authors report a reduction in beam sweeping overhead by as much as 79.3%. [Sim et al., 2020]

Adding to this, a study [Antón-Haro and Mestre, 2019] funded by the European Commission investigated the possibility to conduct beam selection on the uplink using angle-of-arrival in machine learning classification approaches including k-nearest neighbors, support vector classifier and multi-layer perceptron models. Presented results show that the multi-layer perceptron outperformed both other models with results similar to that of theoretically optimal beam selection in terms of sum-rate, which is computed via summation of the achievable bit rates of multiple concurrent transmissions from the analog beamformer.

2

Background

2.1 First Principles of 5G NR

This section describes the first principles deemed necessary to understand connection establishment between a 5G NR Base Station (gNB) and User Equipment (UE). Technical specifications for 5G NR are developed by the 3rd Generation Partnership Project (3GPP) organization.

2.1.1 Introduction

The area of telecommunications is a continuously evolving area of technology which has been an especially hot topic as of late with the first roll-outs of commercial 5G NR networks. This new technology comes with promises of high bandwidth, ultra-reliable and low latency communications and it is expected to assist the development of new technologies such as e-health, connected vehicles and cloud computing. This increase in performance is partially a result of the wavelengths used for transmission, which are shorter than that of previous generations. This is partially enabled by the more advanced beamforming capabilities offered by the 5th generation of mobile networks. [Ericsson, 2022b]

2.1.2 RAN

The Radio Access Network (RAN) is the part of the internet infrastructure that enables over-the-air communication between clients and the core network via radio communication. Examples of clients are mobile phones, computers or any other devices that has the ability to communicate with a base station using radio technology. [Chapter 6 Dahlman, E. and Parkvall, E. and Sköld, J., 2018, Page 73]

2.1.2.1 RAN distribution

Depending on the 5G NR deployment version (3GPP specification), RAN can be realized in several ways. This means that the centralized RAN offers most of its services in a cloud form. If the architecture is not cloud centralized, the aforementioned services are handled by the distributed hardware units in the field. These

units provide the L2 and L3 layer operations and all interconnections between them. [Chapter 6 Dahlman, E. and Parkvall, E. and Sköld, J., 2018, Page 73]

2.1.2.2 Control Plane

RRC in Layer 3 is the main protocol of the control plane. It is responsible for tasks such as cell selection, handover and data conveyance between the user plane layers. Relating back to this thesis, it should be mentioned that the control plane is also responsible for handling beam selection and beam switches performed from the distributed radios in the field. [Flynn, 2022]

2.1.2.3 Carrier Aggregation in the RAN

Carrier Aggregation is a method of assigning multiple carriers (frequency segments) to a user to introduce improvements in terms of throughput. The more frequency segments that are assigned to a user, the more throughput the system is able to enable by utilizing carrier aggregation technology. Using carrier aggregation in the the RAN makes it possible to assign partner bands from different commercial operators for the moving client devices in the cell in order to achieve higher data rates and better coverage. [3GPP, 2022]

2.1.3 Frequency Bands and mmW

The frequency spectrum used in mobile telecommunications is continuously extended as unexploited bands are added with the development of new generations. The range occupied by the different generations do however overlap by design in order to utilize licensed frequency bands efficiently. [Chapter 3 Dahlman, E. and Parkvall, E. and Sköld, J., 2018, Page 31] The physical properties of different frequencies make for different propagation characteristics, with lower frequencies less susceptible to blocking and fading than higher frequencies which can be notably affected even by changes in weather conditions. The long range and high penetrability of low frequency electromagnetic waves come with the downside of lowered bit rate as less information can be encoded into the wave per time unit. Contrarily, higher frequency waves come with the upside of enabling high speeds and low latency, which are both big selling points for the fifth generation mobile networks. The frequency bands are commonly divided into low-band (<1GHz), mid-band (1GHz - 6GHz) and high-band (24GHz - 40GHz). [Chapter 3 Dahlman, E. and Parkvall, E. and Sköld, J., 2018, Page 27] Hardware improvements that led to the possibility of utilizing the high-band frequency range along with the substantial performance increase it implies has prompted a need to further separate and brand the bands. The mid- and low-band range is thus often referred to as the sub-6 GHz bands while high-band has been branded as millimeter wave (mmW) in reference to the wavelengths they use. Limitations in propagation distance of the mmW spectrum have in large been mitigated via advancements in Massive MIMO, miniaturization of antenna processing components and adaptive *beamforming*. [Chapter 3 Dahlman,

E. and Parkvall, E. and Sköld, J., 2018, Page 32]

There are many applications that are utilized by the mmWave frequency bands. Examples of these are radio astronomy, remote sensing, automotive radars defense industry, security in the digital world and telecommunications. [Parker, 2017] Many of the standards that the mmWave spectrum use offer diverse modulation schemes and efficient spectrum manipulation for single or multi-carrier enabling techniques such as Orthogonal Frequency Division Multiplexing (OFDM) and Orthogonal Frequency Division Multiple Access (OFDM-A). MIMO enables Ultra Dense Networks (UDN) to fulfill the need of high capacity without risking a decrease in data rate. UDNs offer better connectivity to the users because of their higher operating frequency, thus the distance between the base stations and the users is decreased. This will enable the networks to become greener since the power consumption will decrease. [Srivastava et al., 2021] MmW is a very popular band of operation, since it enables Device-to-Device (D2D) connectivity. Recently, it has been noticed that more smart devices are using the mmW bands to offer better experience to the users from smart devices other than cell phones, these could either be vehicles, tablets, sensor devices cameras etc. [Zeb et al., 2020]

2.1.4 Reference Signal Received Power (RSRP)

The signal used to measure signal strength in 5G NR is called *Reference Signal Received Power* (commonly RSRP). It is measured in the unit *decibel-milliwatts* and will thus always be a negative number. High RSRP values are desired and the upper theoretical limit is 0. [Chapter 8 Dahlman, E. and Parkvall, E. and Sköld, J., 2018, Page 145]

2.1.5 Synchronization Signal Block (SSB)

The purpose of the SSB is to serve as a container of information that, when broadcasted periodically on the down-link for each beam, enables the UE to locate said beam. This is done through the inclusion of two predefined sequences also stored on the UE called the primary synchronization signal (PSS) and secondary synchronization signal (SSS). Together with the physical broadcast channel (PBCH), these three components constitute the SSB. Like all down-link transmissions in 5G NR, the SSB is transmitted using the modulation scheme OFDM, meaning that it is separated in both time- and frequency domain during transmission.

5G NR was designed with the intent of avoiding so-called always-on signals which are transmitted continuously with short periodicity as time division multiplexing makes such signals block a large number of available slots, considering they are to be sent between gNB and all UEs in the system. Thus, the implementation of the SSB was limited in both transmission periodicity and bandwidth, rendering it less useful for channel sounding on parameters used in beam management as they

can vary rapidly in both time and frequency. Its main use within channel sounding instead lies in measurements of average channel quality and path-loss. [Dahlman, E. and Parkvall, E. and Sköld, J., 2018, Chapter 16]

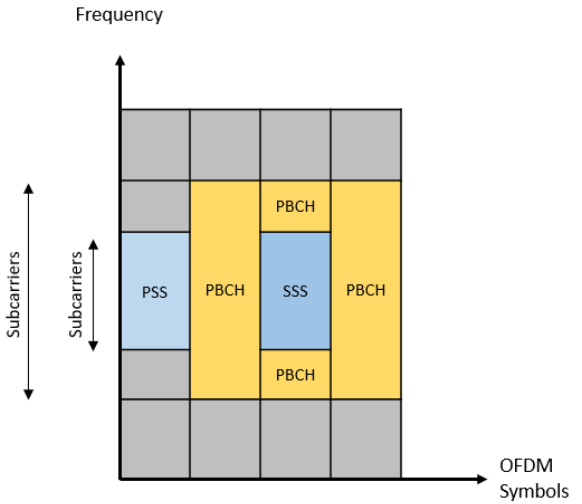

Figure 2.1 Time and frequency domain structure of a Synchronization Signal Block (SSB).

2.1.6 Channel State Information - Reference Signal (CSI-RS)

The main purpose of CSI-RS signals is down-link channel sounding, meaning measurements of parameters linked to the quality of the transmission link. CSI-RS signals are highly configurable in both frequency and time domain, making them flexible and useful for the task of measuring parameters with qualities that impose specific requirements on the sounding signal. These configuration possibilities include splitting the signal over up to 32 different carriers, corresponding to 32 different antenna ports (channels). Actions taken upon receiving a broadcasted CSI-RS signal is configured on a per-device level, meaning that many devices can utilize a single CSI-RS signal in different ways. [Dahlman, E. and Parkvall, E. and Sköld, J., 2018, Chapter 8]

2.1.7 Cell Search

Cell Search is the procedure that is used for identifying individual cells when a UE moves into the area covered by some gNB. It continues to get carried out as the UE moves through the system to maintain updated information about its state, which is necessary to establish and maintain a connection. The Cell Search procedure can be based either on SSBs in both idle and connected state or the channel state infor-

mation reference signal (CSI-RS) in connected state. [Dahlman, E. and Parkvall, E. and Sköld, J., 2018, Chapter 16]

2.1.8 Random Access

The procedure used for establishing a connection between some UE and gNB through a given cell is called Random Access. This procedure consists of four main sub-procedures, namely:

1. UE transmission of a *preamble*
2. gNB transmission of a Random Access Response
3. UE transmission of a message for resolving collisions caused by identical preambles sent by other devices
4. gNB transmission of a follow-up message used to transfer the UE to connected state in case of a successfully resolved collision

Random Access is used when connecting to a cell from idle or disconnected state or when switching to one cell from another. Unlike the rest of the messages, the preamble is sent over a dedicated (physical layer) channel called the Physical Random Access Channel (PRACH) during predefined timing windows determined by the gNB scheduler. The length and periodicity of these dedicated slot windows, also referred to as Random Access Resources (RACH Resources), depend on cell specific characteristics such as size or configured preamble length. The UE bases the transmission timing of a preamble on information derived from a received SSB. [Dahlman, E. and Parkvall, E. and Sköld, J., 2018, Chapter 5]

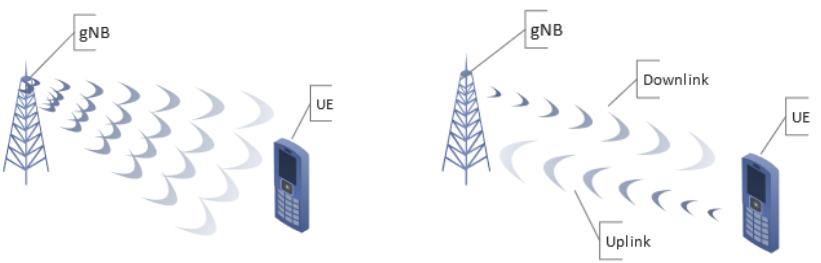

(a) Multiple beams emanating from gNB in multiple directions.

(b) Uplink and downlink beam pair.

Figure 2.2 Images depicting beam forming and beam pairs.

2.1.9 Beam Management

Connection establishment within 5G NR relies heavily on analog beamforming, a technique which aims at establishing and maintaining a suitable beam pair emanating from the gNB and UE correspondingly.

Processing of the analog information received by the antenna of some UE will be performed on a carrier basis. In practice, this means that down-link transmissions from gNB to several UEs at different geographic locations will have to be separated in time, resulting in a so-called beam sweep (sequential transmission over each beam). The same theory holds true for UE side beamforming, meaning that the full system consists of a down-link beam and an up-link beam, hereafter *beam-pair*. Figure 2.2 shows an illustration of beamforming and beam pairs in the system.

The goal of beam management is to continuously maintain a suitable beam pair to support a stable connection between the transmitter and receiver side. The case where a beam pair suitable for down-link transmission is also suitable for up-link transmission is often true. This important quality, often referred to as *beam correspondence*, implies that there is no need to perform the procedure for finding a beam pair from both directions as it is sufficient to perform the necessary computations on one side and assume the result to be valid also for the other side. [Dahlman, E. and Parkvall, E. and Sköld, J., 2018, Chapter 12]

2.1.9.1 Initial Beam Establishment

Beam establishment, meaning for the UE and gNB to agree upon a beam pair, is initialized with gNB performing a beam sweep where SSBs are broadcasted on each beam. Each such SSB carries information such as which beam was used to transmit it and implicit information about the timing window used for preamble transmission. After Random Access has been carried out the network can assume that subsequent transmissions from the UE will be carried out on the same beam used to transmit the preamble. Likewise, the UE can assume that subsequent transmissions from the network will be carried out on the same beam used to transmit the previously received SSB. [Dahlman, E. and Parkvall, E. and Sköld, J., 2018, Chapter 12]

2.1.9.2 Beam Adjustment

The purpose of performing beam adjustment is to improve signal quality by changing either one or both beams in the current pair. The necessity to do so might be rotation or movement of the UE or changes in the environment causing shadowing or reflections. Assuming analog beamforming, the symmetric nature of the up-link and down-link beam pair gives rise to the possibility of either refining the down-link beam direction based on the up-link beam direction or vice versa. [Dahlman, E. and Parkvall, E. and Sköld, J., 2018, Chapter 12]

2.1.9.3 Reporting

The task of selecting a subset of physical channels for communication means that there are two main components relevant to the project: UE and gNB. It is therefore helpful to break down where in the system information is obtained, how it is shared and in what order.

The 5G NR specification makes use of something called report configurations to specify what and how information about the channel state should be collected and reported. More specifically, the report configuration defines the set of quantities to be reported, which exact down-link resources that should be measured to acquire the information and detailed scheduling for up-link transmission of the report. The scope of this project limits the measurement of interest to the received power of a signal (RSRP) transmitted over a certain channel, since this information is vital for beam management. In previous generations of mobile networks, this quantity was measured and transmitted in the network layer, but due to efficiency improvements in 5G NR there is support for reporting RSRP already in the physical layer. The report configuration for the beam management case will thus consist of a set of measurement resources - one SSB per widebeam in the product implementation investigated in this project. The device will then perform measurements on said signals and report the result to gNB to be used by the beam management functionality. [Dahlman, E. and Parkvall, E. and Sköld, J., 2018, Chapter 8]

2.2 First Principles of Machine Learning

This section describes the principles deemed necessary to understand the concept of Machine Learning (ML) along with its possible use cases and limitations.

2.2.1 Introduction

The past decades Machine Learning has been proven to be a very useful methodology to improve the way researchers use and acquire data from real world examples and study cases. The ML scientific era is using algorithms that manipulate different and complex types of data to derive meaningful results that can benefit research and improve the derivation of scientific knowledge. Through knowledge acquisition from complex data helps to expand the understanding of problems unsolved by human capability. Feeding complex and big amounts of data into well performing algorithms can help to apply ML into real world problems and derive even more clever solutions and ways of optimizing resources. [Mitchell, 1997]

2.2.2 Supervised Learning

Supervised learning is the procedure of knowledge acquisition based on example data for output and input. This procedure of supervised learning consists of feeding the system with pairs of inputs. The types of data that the supervised learning

system utilize, consists of training data and validation data which are supposed to be expressed in a numeric fashion. The input data are pairs of training data with a labeled description (in a numeric fashion also). For example, if one would want to classify if an animal is a dog or a cat (see Classification in ML) based on training data, then they would choose 0 and 1 for labels. The procedure of training the system is completed in cycles of training called epochs. The system's performance is hypothetically improving the more epochs it undergoes. The provided data to the system are split into two percentiles. One of the percentiles is fed as training data with which the algorithm creates a mapping of labeled results. The other percentile is given as validation data for the algorithm's results. [Scikit-Learn, 2022c]

2.2.3 Unsupervised Learning

Unsupervised learning shares the same concept of data training as supervised learning, though unsupervised learning feeds the system with unlabeled training data. Since unsupervised learning, works in no labeled data feeding fashion one can notice that it is very difficult for the system to measure its accuracy. Thus, Unsupervised Learning systems tries to make a rationalistic structure, or mapping out, its provided data without any labels. Unsupervised Learning is commonly used to find patterns in data that would have been impossible for humans to find. Data that is uncategorized and non-labeled, which is most likely the data we find for many applications. [Mitchell, 1997]

2.2.4 Balancing of Training Samples for Classification

When gathering training data for any classification machine learning algorithm it is important that samples are evenly distributed across all possible classes. If this is not the case, the model adjustment may become significantly biased towards the more commonly represented classes during training, resulting in poor prediction performance for all underrepresented classes. This can be prevented by undersampling the data such that some samples from the commonly represented classes are removed or over-sampling such that the less represented classes are duplicated through random selection with replacement. A third option is to adjust the cost function such that the impact of a sample during training is weighted according to the inverse of the representation of its corresponding class.

2.2.5 Cross Validation

Cross validation is a practice used to test the performance of an ML model by shuffling and splitting the data used for training and testing. One common way of performing such a split is via the so-called K-fold method, which works by splitting the available data into K groups, where after each group is systematically used as the test set while the rest is used for training. Calculating the prediction score for each of the K test sets then gives good insight into the performance of the model

along with an indication of the level of variability one might expect from a randomly selected training set. [Scikit-Learn, 2022a]

2.2.6 Time Series Forecasting and Supervised Learning

Time series forecasting is the practice of predicting future values of a process using historical, time stamped data. One common approach is to create a mathematical model of the real process through analysis of internal qualities and relationships of the gathered data. Information about the performance of the model can be deduced from the discrepancy between the real process and the values produced by the model, also referred to as the residual, which should ideally be equal to 0 for all sample indices. It is possible to transform a time series forecasting problem to a supervised learning problem by producing labeled data from the historical time series data. For one-step predictions, this is done by letting the values at index n and $n+1$ constitute $\mathbf{X}$ and $\mathbf{y}$ respectively. The traditional method of regression analysis can thus in theory be replaced by a machine learning algorithm trained with labeled data. [Dietterich, 2002]

2.2.7 Training

Generally, the training of an ML model is performed by feeding labeled or unlabeled data into the system based on which internal variables of the model can be adjusted with respect to some cost function. The data type used during training depends on the specific model implementation and the number of iterations and/or samples used depends on a user specified tolerance, processing or time limit.

2.2.7.1 Cost Function

A cost function is a function used to derive a number corresponding to the failure rate of a system. This quantification of inaccuracy is used to set tolerance requirements to be used during training. Since a lower cost means higher accuracy, minimizing the cost function is the fundamental goal of performing training on a given ML algorithm. [Chollet, 2015]

2.2.8 Multi-layer Perceptron (MLP)

A Multi-layer perceptron is a type of artificial neural network which, depending on the implementation, can be used for either binary or multi-class classification and single or multiple output continuous regression. The fundamental structure of the model consists of several layers of nodes, where the first and last one are referred to as the *input layer* and *output layer* correspondingly. In the case of the classification architecture, each output node corresponds to an individual, via training samples seen class. Notably, classification problems with a large sample space does in general require a great and balanced number of training samples to accurately fit a working model. If this requirement is not met, the influence of well represented classes on the fitted model may bury the influence of equally important, but less represented classes. [Scikit-Learn, 2022c]

2.2.9 Random Forest Regressor (RFR)

A Random Forest is a machine learning algorithm consisting of several individual decision trees whose results are weighted together to produce the output of the random forest. Each decision tree consists of a root node, internal nodes and leaf nodes. Each non-leaf node represents categorization in two or more bins based on the value of some variable associated with the node. Each tree is created based on observed data via expansion from the root node where a predefined set of rules define whether or not to perform a given split. [Scikit-Learn, 2022b]

Such rules include:

- A minimum number of samples in a leaf node
- A minimum number of samples needed to perform a split
- The maximum depth of the tree

2.2.10 Convolutional Neural Network (CNN)

A convolutional neural network is a class of a neural network similar to the previously mentioned MLP. The main difference from the other artificial neural networks is the fact that they are able to identify patterns from images passed through several sublayers. The types of sublayers that they use are namely the convolutional layer, the pooling layer and the fully connected layer. The convolutional layer is the main building block of the CNN. In this layer the filtering of multiple overlapping pixels occur in order to map reoccurring features of input images. The pooling layer is where the dimensionality reduction of the CNN occurs as the filter *scans* each input image and select the highest, for extraction, into the next output layer where the average pooling happens. In the fully connected layer, as the name implies, each node in a given layer is connected with the each node in the following one. All together, the CNN model is a neural network capable of performing classification, but modified to accommodate image data types as input [Chollet, 2015] .

2.3 System Modelling

This section describes the first principles deemed necessary to understand parts of the project related to system modelling, including configuration of the simulator environment and attempts at improving the performance of the system through alternative methods of subset selection.

2.3.1 Transition Matrices and Markov Chains

A system which consists of a number of states and the possibility to transition between said states can be represented as a stochastic model in the form of a Markov Chain (see Figure 2.3). This data structure can then be used to simulate the system

behavior by traversing the stochastic graph iteratively. It is common practice to represent a Markov chain as a square matrix, often referred to as a *transition matrix*, where each row and column corresponds to a given state and the values corresponds to the probabilities of transitioning between them. [Chan et al., 2012]

This way, the Markov chain derived from a transition matrix can represent groups of self selected subsets of widebeams that each time stamp of the system progression will give a different possible subset that will supposedly work effectively with the purpose of including the best widebeam measured in RSRP (dBms).

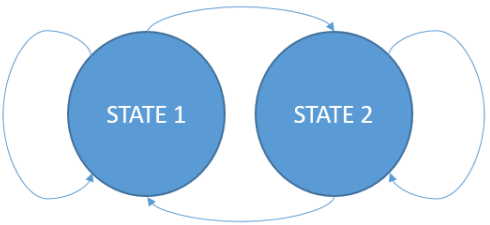

Figure 2.3 A simple example of a Markov chain with two states 1 and 2. The probability of staying in a state is represented as a self-pointing arrow and the probability of transitioning to another state is represented as an arrow pointing away from the current state.

2.3.2 Propagation Model

Signals sent over the air interface in a physical, wireless system experiences undesired effects in the form of decreased amplitude, phase shift and destructive interference. In an effort to understand and counteract these undesired effects, so-called propagation models to be used in simulations have been implemented by 3GPP. [ETSI, 2022] Through models like these, it is possible to study complex phenomena such as the effect of multi-path propagation on a link consisting of multiple bands at different frequencies.

2.3.2.1 Slow Fading Propagation

Fading is considered slow if the rate of change in amplitude and phase shift is slow compared to the minimum delay requirement of the system. The rate of change of the fading is quantified as the *coherence time*, which is the minimum unit of time needed for the amplitude and phase of a channel to change to the degree that it is no longer correlated to its previous value. Ericsson supervisors name shadowing, which can occur due to obstructions in the environment such as a building or hill, as one example of conditions which can introduce slow fading. Furthermore, they add that the slow change in signal properties during the time duration of a typical use case make it possible to model slow fading channels as constant during transmission in simulations. [Belloni, 2004]

2.3.2.2 Spatial Channel Modeling

Due to the high computational cost associated with ray-tracing and low industry demand to simulate a very specific environment very accurately, 3GPP has coordinated the development of a simplified statistical approach, Spatial Channel Modeling (SCM). [ETSI, 2022] It is built on a technique where user locations are considered special points of interest. Objects in the environment, here called *scatterers* are placed randomly in the environment where they are parameterized and associated with each user location. The result is a computationally efficient system with focus on measurements at UE locations. [Ferrand et al., 2016] SCM also includes a specification for simulating propagation to and from antenna arrays used in beamforming. [MathWorks, 2022]

3

Methodology

3.1 Data Gathering

The simulator was set up to simulate a single active user continuously but randomly traversing the area made up by a regular hexagon with a radius of 150 meters (measured from center to vertex) while communicating with the network. The UE was given the task of using the file transfer protocol to transmit a sequence of 100'000 bytes to gNB. Due to the nature of the simulator, a user that has finished its task will despawn and a new instance will be created to fulfill the requirement of keeping a single active user at a given point in time. The final data set used in experiments was gathered throughout 56 minutes of simulated UE and gNB activity.

To achieve the continuous UE movement described above, a new mover type had to be implemented in the simulator source code as no current mover implementation supported the desired functionality. This implementation made it possible to spawn any new user at the last location of the previous one, effectively creating a sequence of RSRP reports that was geographically continuous. This quality was important as the goal of the project involved making predictions based on data gathered in a realistic environment affected by reflections and shadowing. The NLOS model was achieved through simulating a slow fading propagation link with SCM. The radio equipment to be simulated was chosen as a specific, but herein unnamed, commercially available antenna-integrated radio used in deployment of high-band 5G NR networks. This equipment was placed in the bottom vertex of the hexagon, 25 meters above ground level. The user state was automatically set to connected to avoid the RA procedure as this would have slowed down the simulation while not providing any data relevant to the project.

The mover was set to travel around randomly at a speed of 10 km/h and change directions if its next step would have ended up outside the hexagonal area. This way, data points could be gathered homogeneously throughout the radio environment given enough time. Logs for gathering RSRP values for each widebeam were enabled along with logs of the UE position. These outputs from the simulator include undesirable strings and IDs that were removed using MATLAB. A first script

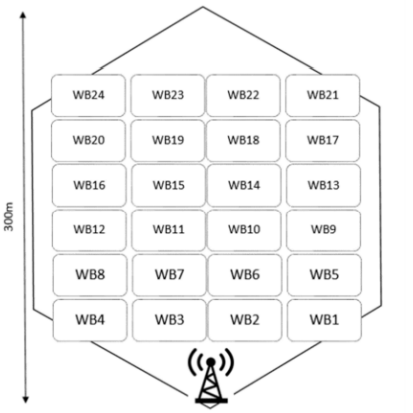

Figure 3.1 Illustration of the hexagonal simulation area and the superimposed theoretical beam grid. As one can imagine, beams directed further away from gNB will occupy a larger area than those close by due to the flashlight effect.

was used to split and sanitize data before creating a comma-separated value file for each log. Plots of the radio environment were also created to provide feedback in the task of tuning the new mover class and verifying that the rest of the simulation was setup correctly.

3.2 Generating Baseline Performance Data

To enable proper evaluation of any algorithms used in this project, it was necessary to quantify the performance of the baseline algorithm. Due to the simulator not supporting the subset functionality at the time of writing the report, an offline version of the baseline algorithm was implemented in *Python* by the authors. In order to ensure this crucial step was performed correctly, both authors implemented their own version separately and the results of feeding the same data into the resulting algorithms were compared and verified by members of a team of baseband developers at Ericsson. The implementation of the baseline was designed such that sanitized logs from the simulator could be fed into the algorithm, essentially simulating the behavior of gNB in the task of handling subset selection while making it possible to track the various KPI mentioned in the previous chapter.

Logging functionality was implemented to track beam miss count, beam switch count, subset switch count, RSRP history and beam history. The ability to track coordinates along with a certain log event was also added to assist in plotting a visual representation of the behavior. This was used to investigate patterns in beam misses.

3.3 Algorithms for Subset Selection

3.3.1 Transition Matrix

The simulated data consists partially of lines of RSRP values for each of the 24 widebeams. To gain further insight into the data set, a matrix keeping track of the number of occurrences where a certain beam went from being the strongest to another one being the strongest, without respect to any subset boundaries, was created. After normalizing each row, the matrix contained the probabilities of each beam having the strongest RSRP in the next measurement given that a certain beam (given by the row number) is currently the strongest. When paired with plots depicting areas where each beam was strongest, this data structure gave insight into how the NLOS propagation model altered the behavior of the system.

The transition matrix serves as a good foundation for experimenting with simple probabilistic approaches for subset selection as the most likely future top beams are easily accessible in each row. It is for example possible to examine the rows recursively to predict which beams will likely become relevant a number of switches into the future.

3.3.2 Markov Chain

In the attempt to dynamically alter the subset of the widebeams that are used from the base station, in order to achieve increased throughput in our channel, endeavors of application of the mathematical system named Markov chains have been made. A Markov chain is a mathematical system that applies a set of probabilistic alterations from different states intertwined. This way it is possible to imitate a probabilistic distribution of alterations depicted as finite discrete states. For the thesis' cause, the finite discrete states are represented by the widebeams that our base station is producing. These are the widebeams 1-24.

As it has been described before, the transition matrix is a graphical representation of the probability distribution of the widebeams alteration. Hence, the finite states of the Markov chain can be represented with a probability vector derived by the transition matrix. Every state of the chain, maps to the other 23 widebeams and also to itself with a certain probability based on the highest RSRP beam in each measurement report [Gallager, 2013]

3.3.3 Random Forest Regressor (RFR)

A multi-input multi-output random forest regressor was trained to predict the RSRP of each widebeam using the RSRP of the last recorded top four beams. The resulting output is then sorted, and the top beams are chosen to constitute the next subset. The training data was structured in such a way that a list of 24 values kept track of the indices of the beams to enable the model to distinguish between them, while the values kept at each index contained the RSRP value for that respective beam. Since only the top four beams are reported back to gNB, all values except four would

therefore have a value of 0. The data used for training was gathered from the big data set described above and extracted such that the top four beams in measurement report *n* constituted **X** and the corresponding RSRP values measured in report *n+1* constituted **y**. Firstly, the training was conducted without any pre-processing, meaning that the four values contained in the training sample lists were the actual RSRP as measured by the device. In an attempt at improving the performance, the values in **X** was also normalized to values between 0 and 1. Since the result of normalizing **X** was not expected, both versions are included in the results section. The training was conducted on a model consisting of 800 decision trees and a maximum number of features equal to the number of samples seen during training.

3.4 Algorithms for Subset Evaluation

The potential of using Machine Learning to validate the subsets was also investigated. The purpose of the subset evaluation experiments is to investigate the viability of evaluating a subset given a full measurement report instead of only the top four beams, which is the result of a design choice rather than a physical limitation in the real world implementation.

3.4.1 Multi-Layer Perceptron Classifier (MLP)

The model used was a Multi-layer Perceptron Classifier, a neural network, which was trained using labeled data created from the recorded subsets (produced by the RFR model) along with the highest RSRP global beam from the corresponding measurement as the label. The input consisted of a list of 24 numeric values, where each index represented a certain widebeam, and the associated value was set to either the recorded RSRP for that beam in case it was included in the subset and 0 otherwise. There were also two hidden layers of 120 and 60 nodes respectively. The output layer consisted of 24 nodes, again corresponding to the beam indexes, of which only one was returned as the predicted highest RSRP global widebeam.

The training data was balanced, meaning to include a similar number of samples for each class during training, through under-sampling to avoid biasing the model towards more commonly represented classes. This reduced the number of samples in the data set from 63239 to 4632 which means a large part of the gathered information was not utilized. The number of epochs used in training was regulated by hyper-parameters such that either a stagnation of improvement (no score improvement of at least 10^{-12} over the last 1k iterations) or a maximum number of iterations (30k) stopped the training procedure.

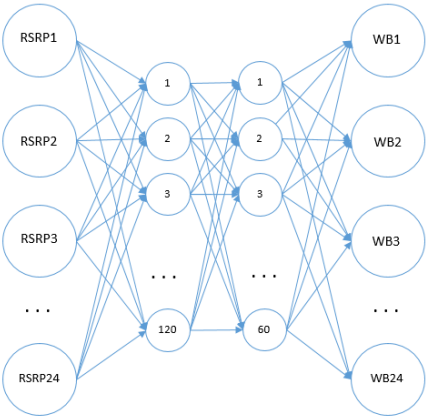

Figure 3.2 Visual representation of the MLP model used for subset evaluation.

3.4.2 Convolutional Neural Network (CNN)

3.4.2.1 Image Production from the subset history

In order to provide input images for the CNN, the subset history from the Markov method was used to create a balanced data set of labeled images with *valid* or *invalid* subsets. The valid subsets are the ones that contained the widebeam with the highest RSRP value in the cell at the time of deployment and the invalid images are the ones that did not. The two sets of subsets were then converted into images representing included and non-included beams. This procedure can be seen in Figure 3.3.

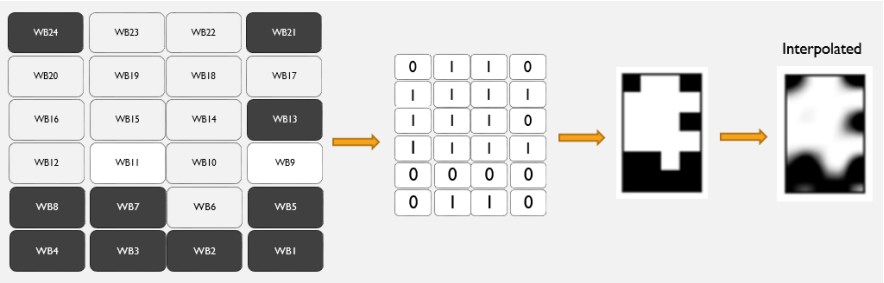

(a) Procedure used to produce the grey scale images.

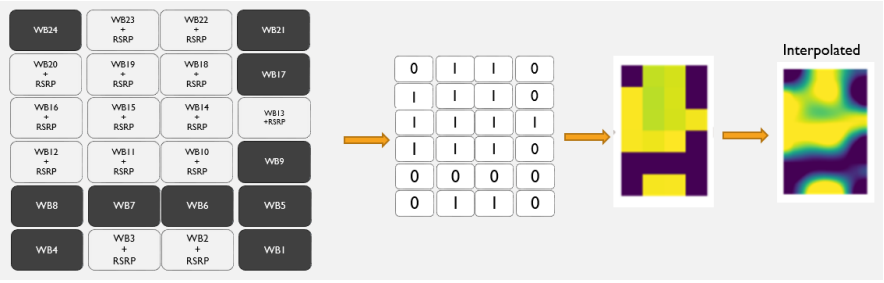

(b) Procedure used to produce the RSRP color coded images.

Figure 3.3 Flow diagrams describing the methodology used to create images to be used in the CNN method from example subset.

Four groups of subset images were produced and used for training. These are shown in the Figures 3.5 - 3.8. In the case of the gray scale images, only the shape of a given subset is encapsulated. The color coded images extend the representation to also account for RSRP strength in each included widebeam, in theory providing a way for the model to relate the user position to the subset shape. Furthermore, a *sinc* interpolation function was used to make the coverage of each subset on the ground surface more realistic. One can notice the effect of the interpolation as non-square subset shapes.

Figure 3.4 Example of gray scale subset without interpolation.

Figure 3.5 Example of gray scale subset with interpolation.

Figure 3.6 Example of RSRP color coded subset without interpolation.

Figure 3.7 Example of RSRP color coded subset with interpolation.

3.4.2.2 CNN Architecture

All four groups of images were used separately in training of the same CNN architecture, which is shown in the Figure 3.8. The specific model implementation used is included in the TensorFlow library. [Martín Abadi et al., 2015]

Layer (type)	Output Shape	Param #
conv2d (Conv2D)	(None, 254, 254, 16)	448
max_pooling2d (MaxPooling2D)	(None, 127, 127, 16)	0
conv2d_1 (Conv2D)	(None, 125, 125, 32)	4640
max_pooling2d_1 (MaxPooling2D)	(None, 62, 62, 32)	0
conv2d_2 (Conv2D)	(None, 60, 60, 16)	4624
max_pooling2d_2 (MaxPooling2D)	(None, 30, 30, 16)	0
flatten (Flatten)	(None, 14400)	0
dense (Dense)	(None, 256)	3686656
dense_1 (Dense)	(None, 1)	257

Figure 3.8 Convolutional neural network architecture.

3.4.2.3 Training of the CNN

The training was conducted by feeding the CNN with batches of 32 images out of a pool of 724 equally classified images from classes of valid and invalid subsets from the Markov method. The four groups of images were each used in training over 25 epochs. The data set of each group was divided in 70% training data, 20% validation data and 10% testing data. The average accuracy of the classification prediction was calculated using 5-fold cross validation.

4

Results

4.1 Simulator Configuration

The configuration of the radio environment simulation was verified by studying Figure 4.1 which depicts the propagation of 8 beams from gNB with LOS enabled, meaning via slow fading propagation without SCM. It is clear that the beams propagate in the directions predicted by the theoretical beam grid used in the product. Comparing Figures 4.1 and 4.2 gives good insight into how the slow fading propagation model with SCM affects the radio environment as the directions of left angled beams seem to be fairly intact apart from increased internal noise, while right angled beams appear to reflect of a scatterer close to gNB. Widebeam 17, which is intended to connect with the upper right part of the hexagon, is scattered but mainly reflected to the left hand side instead. Widebeam 1, which is intended to connect with an area to the right hand side of and close to gNB is almost completely blocked.

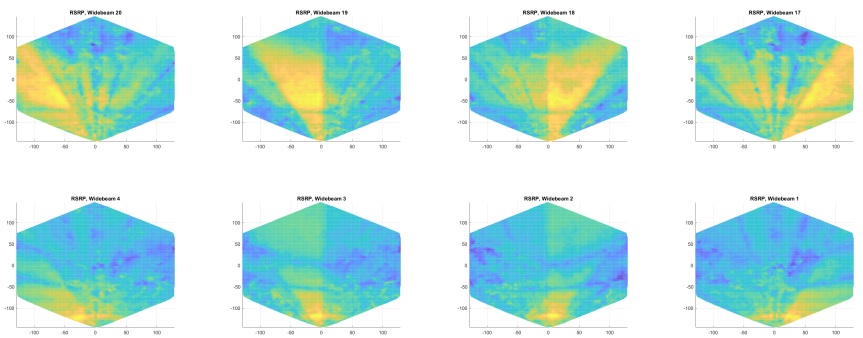

Figure 4.1 Plot of RSRP values per widebeam from a LOS simulation.
Top row: WB20, WB19, WB18, WB17. Bottom row: WB4, WB3, WB2, WB1. It is clear that the beams propagate in the expected direction based on the theoretical beam grid.

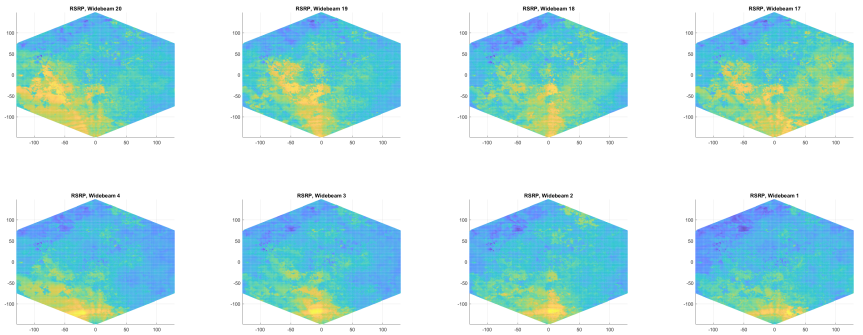

Figure 4.2 Plot of RSRP values per widebeam from an NLOS simulation.
Top row: WB20, WB19, WB18, WB17. Bottom row: WB4, WB3, WB2, WB1. The theoretical grid is mostly intact on the left hand side, but very distorted on the right hand side.

4.1.1 User Movement

The behavior of the UE mover class implemented by the authors to generate a geographically continuous random trail in the simulation area is presented below. Figure 4.3a shows the geographical position associated with each measurement report gathered during a relatively small time frame in order to properly distinguish the characteristics of the movement. Figure 4.3b, which contains 63239 samples, shows the geographical positions associated with all measurement reports contained in the big data set used for experiments.

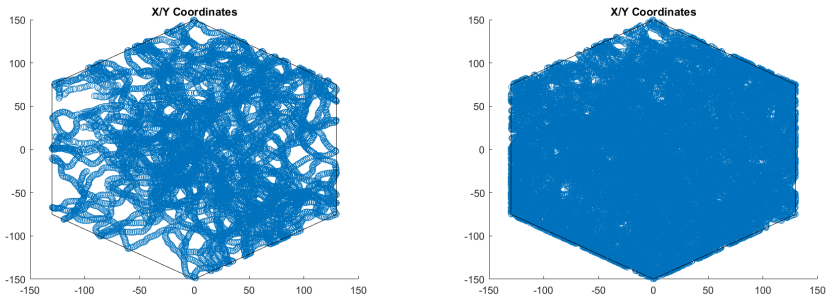

(a) Visual example of the trail generated by the modified random mover.

(b) Coordinates from all samples in the data set used for experiments.

Figure 4.3 Coordinate locations depicting the random mover behavior.

4.2 Data Gathering

During the simulation, the UEs location and measured RSRP was logged as it traversed the NLOS radio environment surrounding gNB. Figures 4.4a and 4.4b shows the geographical coordinates (x,y) associated with each measurement report in a 3-dimensional space with z corresponding to the beam index with highest measured RSRP. In the LOS case, each beam is clearly mapped to a specific geographical area corresponding to the theoretical beam grid. The NLOS plot shows a similar result at lower index beams close to gNB where a clear separation between the layers is maintained. The noise introduced by the propagation model becomes a lot more apparent at medium to high index beams as vertical outliers increase remarkably in numbers and the borders between layers become increasingly undefined, especially on the right hand side where an object close to gNB appears to be interfering significantly with the beams.

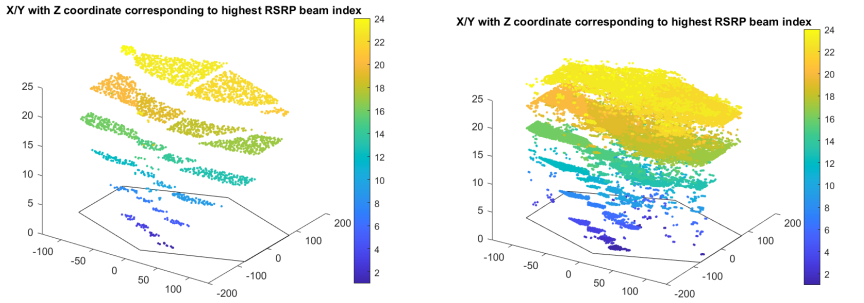

(a) LOS simulation with datapoints sorted vertically depending on the highest RSRP beam. There is distinct separation between beams at different coordinates which is expected on a flat surface.

(b) NLOS simulation with datapoints sorted vertically depending on the highest RSRP beam. The environment has introduced noise into the system, but the theoretical beam grid can still be visible especially at lower index beams close to gNB.

Figure 4.4 Comparing RSRP measurements in LOS and NLOS.

4.3 Beam Switch Transition Matrix

Figure 4.5 depicts the transition matrix generated by tracking the beam index of the highest RSRP beam in each measurement report. The matrix, which is of dimensions 24x24, should be interpreted such that a row index corresponds to the current strongest beam and each of the values of that row contains probabilities of each of the other beams being the strongest in the following measurement report. The ma-

trix has a strong diagonal, meaning that the on average most likely event is that the current strongest beam is also the strongest beam in the next measurement report.

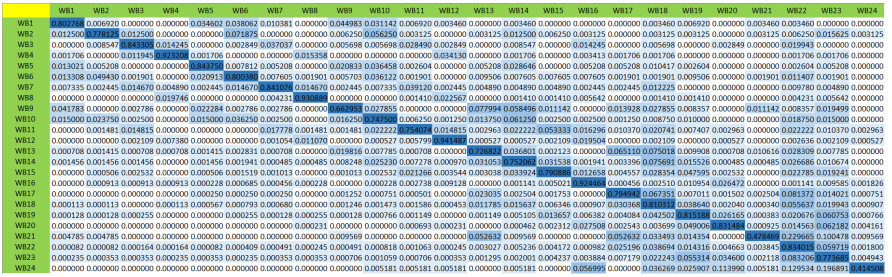

Figure 4.5 Transition matrix generated by tracking beam switches throughout the big dataset used in experiments.

4.4 Baseline Performance

Running the RSRP measurement reports generated by the simulator configuration above through the python implementation of the currently used static subset algorithm generated what is also referred to as the baseline performance. This performance serves as a benchmark for all following alternative methods. Table 4.1 shows that roughly every 10th beam switch results in a subset switch and that 728 beam misses occurred in total over the 56 minutes of simulated time (0.2162 misses/s), meaning that 6.3% of all beam switches resulted in a miss. Figure 4.6 shows the coordinates of said misses. Most misses occur close to gNB and in series which could be partially explained by the small area covered by each low index beam due to propagation distance. Furthermore, a significant portion occur close to the middle of the hexagon, which is expected since this corresponds to the location where the four static subsets overlap.

Baseline	
Beam Switches	11573 (3.4362 switch/s)
Subset Switches	1172 (0.3480 switch/s)
Beam misses	728 (0.2162 miss/s)
Average RSRP (dBm)	-103.291

Table 4.1 Baseline performance.

4.4.1 KPI performance of the Optimal Selector

In order to put the performance achieved by the alternative methods presented below into perspective, the average RSRP of a hypothetical, optimal method which

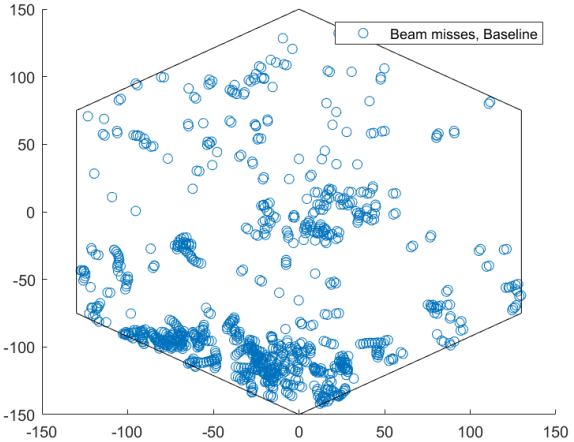

Figure 4.6 Coordinates where a beam miss occurred when using the Baseline Selector.

would always include the best beam (meaning 0 beam misses) in each subset was calculated as -102.495 dBm, meaning that these are the respective upper and lower bounds which can be achieved on the data set used in experiments. The lowest theoretical number of beam switches required for a given data set is found by counting the number of instances of two consecutive reports where the two corresponding highest RSRP values map to different beams. The number is however not independent from the subset selector as the UE can only detect a required beam switch within the assigned subset. For the optimal subset selector which always includes the best beam, the optimal beam switch count is 11592. The minimum number of subset switches which could be achieved remains unknown.

4.5 Alternative Methods for Subset Selection

In this section, the KPI of the Markov method and Random Forest Regressor selectors are presented.

4.5.1 Markov Method

The Markov method yielded very good results in terms of beam misses compared to the baseline, but suffers in the subset switches metric as it is very unlikely that two identical subsets are chosen randomly twice in a row. The locations of the beam misses are presented in Figure 4.7. Notably, the misses are much less dense around gNB and the tendency for misses to be consecutive, as is the case in the baseline, is not present in this selector. [Gallager, 2013]

Markov Method	
Beam Switches	11625 (3.4516 switch/s)
Subset Switches	58960 (17.51 switch/s)
Beam misses	348 (0.1033 miss/s)
Average RSRP (dBm)	-102.506

Table 4.2 Markov methodology performance.

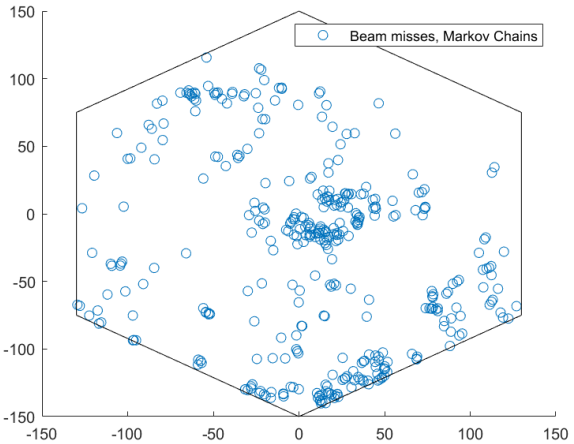

Figure 4.7 Coordinates where a beam miss occurred when using the Markov selector method.

4.5.2 Relation Between Subset Size and Beam Misses

The relation between different subset sizes and beam misses were also investigated for the Markov method. As expected, bigger subset sizes result in less beam misses than smaller ones. Figure 4.8 shows an exponential decrease in beam misses with an increasing subset size. Trivially, a subset of size 24 (meaning to include the full cell) results in 0 beam misses.

4.5.3 Random Forest Regressor (RFR)

The performance of replacing the baseline subset selection procedure with that generated by the Random Forest Regression model is presented in Tables 4.3 and 4.4. The unscaled input performed better than the scaled input but both performed better than the baseline algorithm in terms of beam misses (5.55% and 5.67% of beam switches resulted in a beam miss respectively). The number of subset switches is roughly 10 times that of the baseline for both the scaled and unscaled versions.

The geographical locations where a beam miss occurred is presented in Figures 4.9a and 4.9b respectively. The bulk of the misses occur in the immediate area

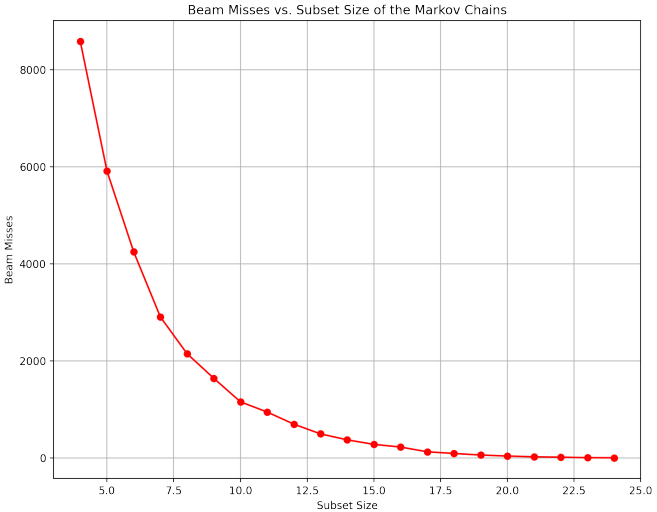

Figure 4.8 Relation between subset size and beam misses in the Markov method.

surrounding gNB, but the misses are spaced more uniformly around the station as opposed to being biased to the left hand side as was the case with the baseline algorithm. The cluster of misses close to the center of the hexagon is reduced compared to the baseline, but still present.

RFR Selector (unscaled input)	
Beam Switches	11564 (3.4335 switch/s)
Subset Switches	11528 (3.4228 switch/s)
Beam misses	642 (0.1906 miss/s)
Average RSRP (dBm)	-102.545

Table 4.3 RFR Selector (unscaled input).

RFR Selector (scaled input)	
Beam Switches	11554 (3.4276 switch/s)
Subset Switches	11520 (3.4204 switch/s)
Beam misses	656 (0.1948 miss/s)
Average RSRP (dBm)	-102.541

Table 4.4 RFR Selector (scaled input).

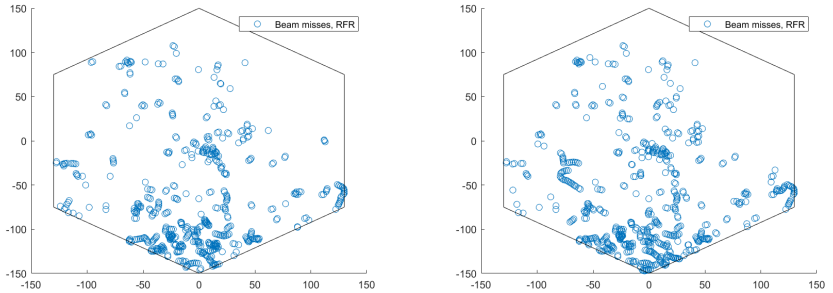

(a) Coordinates where a beam miss occurred when using the RFR Selector with unscaled input.

(b) Coordinates where a beam miss occurred when using the RFR Selector with scaled input.

Figure 4.9 Coordinates for beam misses in the RFR Method.

4.6 Alternative Methods for Subset Evaluation

The abilities of the MLP classifier and CNN classifier to evaluate whether a given subset included the strongest beam or not were also investigated.

4.6.1 Multi-Layer Perceptron Classifier (MLP)

The MLP method of evaluation resulted in an average 76.8% prediction accuracy, calculated using 5-fold cross-validation. Under-sampling, which was utilized to balance the classes prior to training, resulted in 4632 of the original 63239 samples to be used during training. Figure 4.10 shows the confusion matrix of the relation between predicted and actual labels. Notably, the two vague diagonal lines above and below the true diagonal show that the most common misclassification happen as a result of the model predicting the widebeam directly above or below the correct widebeam in the theoretical beam grid.

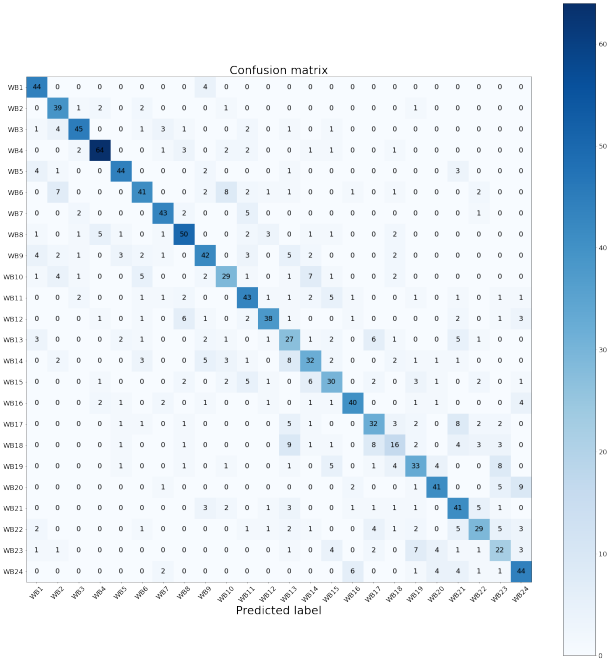

Figure 4.10 Confusion matrix from the MLP evaluator model. X-axis and Y-axis shows the predicted beam and actual beam.

4.6.2 Convolutional Neural Network (CNN)

The trained CNN model was able to evaluate whether or not a given subset generated by the Markov method included the highest RSRP widebeam in the cell or not at a notably high accuracy. The grey-scale image representation of the subsets yielded results of 75% accuracy both in interpolated and non-interpolated version. The RSRP color coded versions increased the accuracy to 81.3% and 95.3% respectively as can be seen in Table 4.5. Thus, it seems that the preprocessing step of smoothing the subset edges had a bigger impact on the performance of subset images that included an RSRP component than those that did not. [Chollet, 2015]

Average accuracy rate	
Gray-scale without interpolation	74.0%
Gray-scale with interpolation	75.0%
Colored without interpolation	81.3%
Colored with interpolation	95.3%

Table 4.5 Average accuracy rate of the different image groups used in the CNN method.

4.7 Summary

Figures 4.11, 4.12, 4.13 and 4.14 show the performance of each method for each respective KPI. The Markov method is noteworthy for its low beam miss count of 0.1033 misses per second (baseline: 0.2162) and very high subset update cost due to updating the subset at nearly every opportunity, meaning 17.5 times per second (baseline: 0.3480). The RFR method presents a less costly smaller improvement in beam misses at 0.1906 misses per second at a cost of 3.4228 subset updates per second. The average RSRP of the baseline, -103.29 dBm, is already close to the theoretical optimum of -102.49 dBm, but both alternatives pushes the performance exceptionally close to the limit at -102.51 dBm for the Markov method, -102.55 dBm (unscaled) and -102.54 dBm (scaled) for the RFR method.

The number of beam switches is very similar between the baseline and all presented alternative methods, which is partially expected since the update criterion is based on the strongest measured beam in each measurement report, which is the same for all methods. The small differences are a result of the included beams in each subset since only beams within the assigned subset are included in the comparison between the previously best and currently best beam.

The location of the beam misses for each respective method differs notably from the baseline which experiences problems with consecutive misses across the lower part of the hexagon and especially in the area immediately surrounding gNB. The Markov method successfully addresses the issue of consecutive beam misses, with the coordinate pattern seeming more random and spread out except from in the middle of the hexagon where most of the misses occur. Especially notable is the area close to gNB which was where the majority of misses occurred in the baseline. The RFR method still results in some chains of consecutive misses and the main issues lie close to gNB, although more uniform around gNB in the area corresponding to beams 1-4.

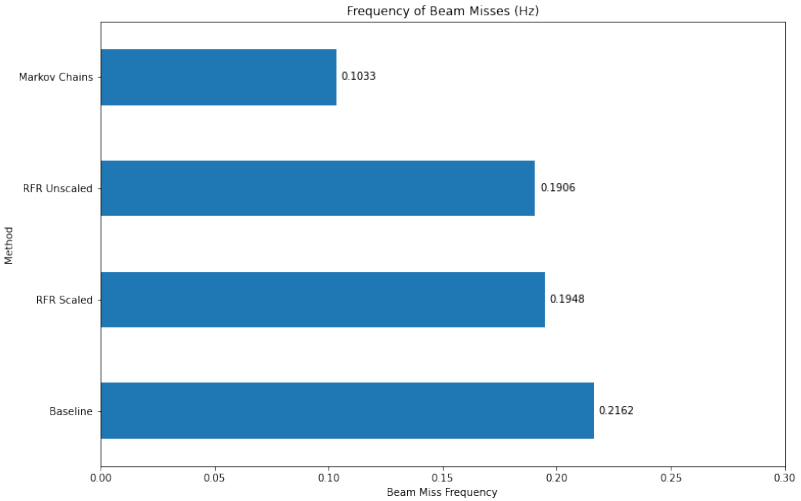

Figure 4.11 Number of beam misses of the respective methods used for subset selection.

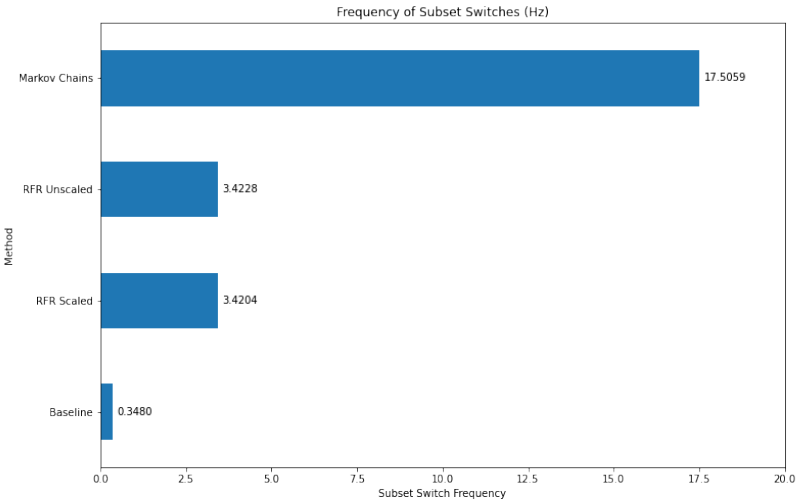

Figure 4.12 Number of subset switches of the respective methods used for subset selection.

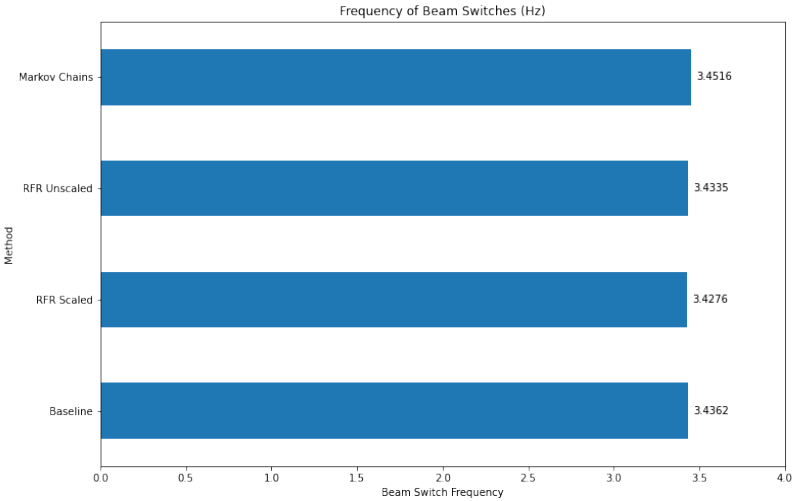

Figure 4.13 Number of beam switches of the respective methods used for subset selection.

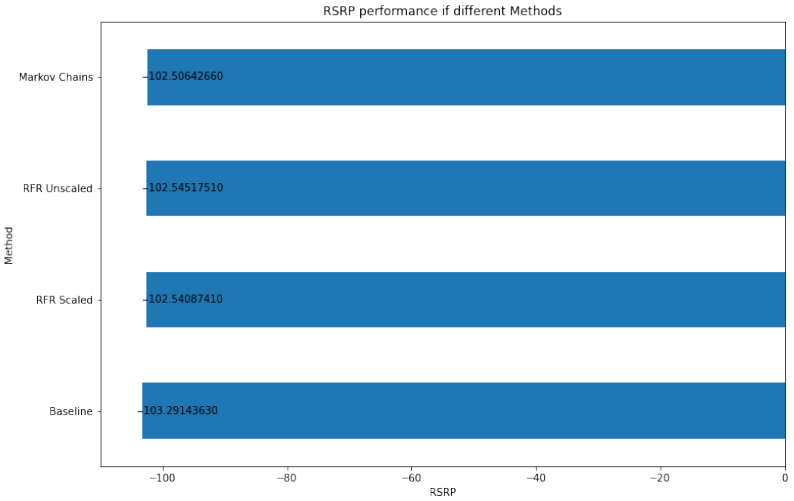

Figure 4.14 Average RSRP of the respective methods used for subset selection.

5

Discussion

5.1 Interpreting the Key Performance Indicators (KPIs)

The subset switch count is an important metric of performance in the use-case investigated in this project, but it is important to remember that this only applies to systems where updating the currently serving subset comes at a significant cost of some kind. Since RAN systems are distributed, any information relevant to two communicating components (e.g., gNB and UE) need to propagate over the air interface, which costs resources in the form of time slots (time division multiplexing blocks all but one transmission from gNB at a given time instant) and processing power (clock cycles, battery power). Notably, energy is of especially high value in battery powered devices. Furthermore, it should be noted that a real-world implementation of a solution driven by a machine learning model requires continuously evaluating a prediction function and possibly also updating the model periodically to adjust for changes in the radio environment caused by the likes of construction sites and changes in weather conditions. The average RSRP measured by the UE gives a good indication of the performance of the solution over time but does not effectively capture temporary disturbances like loss of connection or otherwise unstable performance which is crucial for the end consumer. The beam miss metric is determined by supervisors at Ericsson to be the most significant indicator of a subset selection algorithm as it quantifies the performance directly related to the purpose of the beam subsets – seeking to ensure that the user is connected to the most appropriate beam at all times at the lowest possible cost.

5.1.1 Properties of the Simulation Data Used In Experiments

The data set used in experiments is gathered uniformly throughout the hexagonal area which means that beams far away from gNB, which naturally cover a larger area, was measured as the strongest beam in more instances than those closer to gNB. This is a true property of the real system and not a result of poor practice when gathering the data, and is thus not a problem when using it for subset selection. However, in the case of subset evaluation, where the classification model was

trained to identify the strongest global beam based on a full subset measurement report, balancing is needed to avoid over-fitting the model to the classes corresponding to the over-represented, higher index beams.

The transition matrix was created in order to access the probabilities of all possible beam switches in the environment. Notable properties that were found include:

- Staying on the same beam multiple measurements in a row is the most common scenario for all beams.
- It is uncommon to switch directly from a high index beam to a low index beam and vice versa.
  - This, together with results presented in Figures 4.4a and 4.4b indicate that the theoretical beam grid stays notably intact even after introducing noise through the NLOS propagation model.
- Some switches would never occur within the simulated period due to the way the radio environment affected the data.

Certain non-existent switches were expected to some extent as it is plausible that the propagation model would completely block certain beams of the radio environment from ever neighboring in RSRP value. It was however more surprising that the geographical neighbors in the theoretical beam grid resulting from the propagation model would be a good predictor of RSRP neighbors even after interference from the propagation model, but it does give insight into why the naive baseline implementation worked as well as it did compared to the more advanced methods. It should be noted that it is possible that the seed used in the simulation affects the propagation less than the average real-world deployment or other simulation seeds. Due to the limited scope of the project, this hypothesis is left as a possibility to further develop the study in the future.

5.2 Subset Selection and Evaluation Approach

With the ultimate goal of the project being to develop a system that was able to effectively select subsets that would increase performance, it was decided to explore self-correcting behavior to avoid chains of repeated bad selections. The idea of an evaluation mechanism encouraged the development of a modular algorithm consisting of a selector, metadata-selector and evaluator in a feedback loop including an exit routine that could reset the state of any memory dependent selector model. The intended purpose of the metadata-selector concept is to use the information received by the evaluator to adjust state variables used in the following creation step, effectively offloading responsibility from the selector to reduce model complexity.

Suggested functionality of the metadata-selector includes estimating subset size and the UEs direction of movement. The subset size is, based on tests showing

the performance of the Markov method for different subset sizes, believed to be a crucial parameter for reducing the average power required to process each subset. However, answering this question requires proof that there can exist an algorithm which can determine appropriate low-risk time instants where the size can be reduced without causing a severe reduction in performance. A previous project conducted at Ericsson which investigated the possibility of improving signal strength of a moving UE, such as a car passenger, concluded that the direction of travel is useful as it can be used to assign weights to beams depending on velocity and direction of travel. [Patel et al., 2020]

This modular approach also enables the possibility of having multiple parallel selectors that are executed based on parameters found in the evaluation steps. It is plausible that the results from multiple parallel evaluators could yield information used to switch between a range of specialized selectors depending on the previous user and subset states. Such states could in practice be related to the UEs means of transport or varying weather conditions.

5.2.1 Comparing the Methods of Subset Selection

Two algorithms were developed with the intent of selecting a subset based on data gathered from the environment. The first one, the Markov method, is based upon the statistical behavior of the system in terms of beam switches. The second one, the RFR method, is performing selection based on time series forecasting performed by a supervised ML model.

In the case of the Markov method we can notice a significant decrease in beam misses compared to the other methods used. This statistical approach works more efficiently than the previously used baseline subset selection algorithm and both version of the RFR selector. One can see a drop of nearly 46% in terms of beam misses, which is not very surprising since the update frequency of the subsets in the Markov method is vastly higher than that of all other investigated methods.

5.2.2 Comparing the Methods of Subset Evaluation

By examining the plots showing where beam misses occurred geographically it can be concluded that a big part of them occur in sequence, which highlights a weakness in both the baseline, Markov and RFR method. All algorithms are blind in the sense that they do not include routines for adjusting to the quality of previous outputs. While it would likely be possible to modify it to incorporate such functionality, the authors concluded that there is merit to delegating the evaluation to a separate module since this approach would enable the selector and evaluator to be improved or replaced individually.

The choice of letting the evaluator have access to the full subset measurement was based on the fact that the current limitation of only including the RSRP of four beams in the report is not a system limitation, but a design choice. The subset functionality, being already present in the product, motivates exploring selection meth-

ods compatible with the current report configuration. Following the same reasoning, limiting evaluation experiments to be compatible with the current configuration was not deemed constructive as the concept of evaluation is not currently a part of the system. If such a feature was to be added, it is expected to be relevant further in the future relative to an update to the subset selection procedure, according to baseband engineers at Ericsson.

5.2.3 Training Data used in RFR and CNN

The RFR was trained with RSRP measurements gathered from the UE as it traversed the simulation area. Similarly, the CNN was trained using subset history produced from the Markov method. In theory, this introduces a bias in the data corresponding to the UEs direction of movement. However, due to the frequency at which measurements and reports are transmitted between the UE and gNB, combined with the accuracy at which the current product is able to calculate the user position, it was decided that including a directional component was not necessary. This hypothesis was strengthened in the results which show an improvement in beam misses compared to the baseline in the case of the RFR method, which indicates that the model is able to provide a useful (although noisy) estimation of future RSRP reports without information related to the UE's direction of movement. Likewise, the CNN is able to evaluate whether or not the highest RSRP beam in the cell is present in a given subset or not at significant accuracy of up to 95.3%.

5.3 Future Work

5.3.1 Introducing Biases from the Beam Grid

The quadrants in the transition matrix shows a clear pattern that lower and higher index beams are much more likely to switch a beam in their corresponding group. Switches from higher index beams to lower index beams and vice versa are both unlikely, potentially explaining why the static subset layout performed as well as it did in terms of beam misses. Since the theoretical beam grid layout stays partially intact in experiments, manually biasing the matrix according to the cell setup might be a way to improve performance in future implementations. The authors believe the goal of such an experiment should be to search for optimal bias weights, possibly by recording the performance of the Markov method for each combination of a range of bias values crossed with a range of simulator seeds.

5.3.2 Testing the Evaluation Hypothesis

The pre-study on evaluators presented in this report suggests that it is indeed possible to evaluate the quality of a subset, which opens up the possibility to create a more intelligent system that includes feedback between the selector and evaluator. The authors envision a project on this topic to include experiments on the effect

of introducing noise into the system and altering the input to the selector such that the output of the evaluator could affect the next output in a constructive direction if deemed necessary. Additionally, quantifying such a system in terms of the KPI used in this project would serve as an interesting, complementary, future study.

Another thing to consider is the the fact that users do not generally move randomly in the real world as organized pathways and infrastructure heavily restricts and influences movement. The uncertainty posed by a random direction of travel is also assumed to introduce a certain level of unrealistic noise into the system. It should therefore be mentioned that any prediction algorithms used in this thesis could in theory benefit from being trained using data gathered through more realistic, non-random user movement.

Bibliography

3GPP (2022). *Carrier aggregation explained*. URL: https://www.3gpp.org/technologies/keywords-acronyms/101-carrier-aggregation-explained.

Antón-Haro, C. and X. Mestre (2019). "Learning and data-driven beam selection for mmwave communications: an angle of arrival-based approach". *IEEE Access* **7**, pp. 20404–20415. DOI: 10.1109/ACCESS.2019.2895594.

Belloni, F. (2004). *Fading Models*. Tech. rep. S-88 Signal Processing Laboratory, HUT.

Chan, K., C. Lenard, and T. Mills (2012). *An Introduction to Markov Chains*. Tech. rep. The MAV 49th Annual Conference. La Trobe University, Bundoora, VIC, Australia. DOI: 10.13140/2.1.1833.8248.

Chollet, F. (2015). *Keras*. URL: https://github.com/fchollet/keras.

Dahlman, E. and Parkvall, E. and Sköld, J. (2018). *5G NR : The Next Generation Wireless Access Technology*. Academic Press, an imprint of Elsevier.

Dietterich, T. G. (2002). "Machine learning for sequential data: a review". In: *Structural, Syntactic, and Statistical Pattern Recognition*. Springer Berlin Heidelberg, Berlin, Heidelberg, pp. 15–30.

Ericsson (2022a). *How 3gpp is setting the security standards for a 5g future*. Last accessed May 23rd 2022. URL: https://www.ericsson.com/en/blog/2020/5/3gpp-security-standards-5g-future.

Ericsson (2022b). *What is 5g?* Last accessed May 23rd 2022. URL: https://www.ericsson.com/en/5g?gclid=EAIaIQobChMI9drL3tz19wIVC7vVCh2IVQa3EAAYASAAEgJH1_D_BwE&gclsrc=aw.ds.

ETSI (2022). *5g; study on channel model for frequencies from 0.5 to 100 ghz (3gpp tr 38.901 version 17.0.0 release 17)*. Last accessed May 10th 2022. URL: https://www.etsi.org/deliver/etsi_tr/138900_138999/138901/17.00.00_60/tr_138901v170000p.pdf.

Ferrand, P., M. Amara, S. Valentin, and M. Guillaud (2016). "Trends and challenges in wireless channel modeling for evolving radio access". *IEEE Communications Magazine* **54**:7, pp. 93–99. DOI: 10.1109/MCOM.2016.7509384.

Flynn, K. (2022). *Control and user plane separation of epc nodes (cups)*. URL: https://www.3gpp.org/cups.

Gallager, R. G. (2013). *Stochastic Processes Theory for Applications*. Cambridge University Press, 2013.

Martín Abadi, Ashish Agarwal, Paul Barham, Eugene Brevdo, Zhifeng Chen, Craig Citro, Greg S. Corrado, Andy Davis, Jeffrey Dean, Matthieu Devin, Sanjay Ghemawat, Ian Goodfellow, Andrew Harp, Geoffrey Irving, Michael Isard, Y. Jia, Rafal Jozefowicz, Lukasz Kaiser, Manjunath Kudlur, Josh Levenberg, Dandelion Mané, Rajat Monga, Sherry Moore, Derek Murray, Chris Olah, Mike Schuster, Jonathon Shlens, Benoit Steiner, Ilya Sutskever, Kunal Talwar, Paul Tucker, Vincent Vanhoucke, Vijay Vasudevan, Fernanda Viégas, Oriol Vinyals, Pete Warden, Martin Wattenberg, Martin Wicke, Yuan Yu, and Xiaoqiang Zheng (2015). *TensorFlow: large-scale machine learning on heterogeneous systems*. URL: https://www.tensorflow.org/.

MathWorks (2022). *Simulate channel models for wireless systems*. Last accessed May 10th 2022. URL: https://se.mathworks.com/discovery/channel-model.html.

Mitchell, T. M. (1997). *Machine learning*. McGraw-Hill New York.

Parker, M. (2017). *Automotive radar with contributions by ben esposito. digital signal processing 101*. URL: https://www.sciencedirect.com/topics/engineering/automotive-radar.

Patel, B., P. Fryking, H. Schang, and J. Hou (2020). *Determination of candidate set of beams for beam tracking*. Ericsson AB Patent Application. International Patent Application Number: PCT/EP2019/064569.

Scikit-Learn (2022a). *Cross-validation: evaluating estimator performance*. Last accessed May 4th 2022. URL: https://scikit-learn.org/stable/modules/cross_validation.html.

Scikit-Learn (2022b). *Ensamble methods*. Last accessed June 3rd 2022. URL: https://scikit-learn.org/stable/modules/ensemble.html#forests-of-randomized-trees.

Scikit-Learn (2022c). *Neural network models (supervised)*. Last accessed August 26th 2022. URL: https://scikit-learn.org/stable/modules/neural_networks_supervised.html.

Sim, M. S., Y.-G. Lim, S. H. Park, L. Dai, and C.-B. Chae (2020). "Deep learning-based mmwave beam selection for 5g nr/6g with sub-6 ghz channel information: algorithms and prototype validation". *IEEE Access* **8**, pp. 51634–51646. DOI: 10.1109/ACCESS.2020.2980285.

Srivastava, A., M. S. Gupta, and G. Kaur (2021). “Chapter 1 - impact of artificial intelligence on future green communication”. In: Kaur, G. et al. (Eds.). *Artificial Intelligence to Solve Pervasive Internet of Things Issues*. Academic Press, pp. 1–12. ISBN: 978-0-12-818576-6. DOI: https://doi.org/10.1016/B978-0-12-818576-6.00001-0. URL: https://www.sciencedirect.com/science/article/pii/B9780128185766000010.

Wang, B. (2021). *Adaptive Beam Management in 5G-NR: A Machine Learning Perspective*. Tech. rep. Faculty of Engineering, Lund University.

Zeb, S., A. Mahmood, H. Pervaiz, S. A. Hassan, M. I. Ashraf, Z. Li, and M. Gidlund (2020). “On toa-based ranging over mmwave 5g for indoor industrial iot networks”. In: *2020 IEEE Globecom Workshops (GC Wkshps*, pp. 1–6. DOI: 10.1109/GCWkshps50303.2020.9367555.